Co-Kriging Method for Form Error Estimation Incorporating Condition Variable Measurements

Shichang Du[1]
State Key Lab of Mechanical System and Vibration,
Shanghai Jiaotong University,
Shanghai 200240, China;
Department of Industrial Engineering and Management,
School of Mechanical Engineering,
Shanghai Jiaotong University,
Shanghai 200240, China

Lan Fei
Department of Industrial Engineering and Management,
School of Mechanical Engineering,
Shanghai Jiaotong University,
Shanghai 200240, China

The form error estimation under various machining conditions is an essential step in the assessment of product surface quality generated in machining processes. Coordinate measuring machines (CMMs) are widely used to measure complicated surface form error. However, considering measurement cost, only a few measurement points are collected offline by a CMM for a part surface. Therefore, spatial statistics is adopted to interpolate more points for more accurate form error estimation. It is of great significance to decrease the deviation between the interpolated height value and the real one. Compared to univariate spatial statistics, only concerning spatial correlation of height value, this paper presents a method based on multivariate spatial statistics, co-Kriging (CK), to estimate surface form error not only concerning spatial correlation but also concerning the influence of machining conditions. This method can reconstruct a more accurate part surface and make the estimation deviation smaller. It characterizes the spatial correlation of machining errors by variogram and cross-variogram, and it is implemented on one of the common features: flatness error. Simulated datasets as well as actual CMM data are applied to demonstrate the improvement achieved by the proposed multivariate spatial statistics method over the univariate method and other interpolation methods. [DOI: 10.1115/1.4031550]

Keywords: quality control, form error estimation, multivariate spatial statistics, co-Kriging, coordinate measuring machine

1 Introduction

Surface form is predominantly considered as one of the most important features of practical product surfaces due to its crucial influence on the functional behavior of a machined part [1–8]. The form error estimation under various machining conditions is an essential step in the assessment of part surface quality generated in machining processes [9]. In order to estimate form error, the general approach is to fit a set of discrete measurement points to an underlying model to obtain an artificial surface and calculate the magnitude of form error. CMMs are widely used as an excellent measurement equipment due to its accuracy and versatility in measuring complicated geometries [10,11]. Considering measurement cost, only a few measurement points are collected offline using a CMM for a part surface in mass production. On the other hand, with the development of new advanced machining condition measurement equipments, a lot of machining condition data can be available online. Therefore, fitting an artificial surface with a more accurate representation of the actual surface using the finite offline sample points and lots of online measurement data is of great importance under certain machining conditions.

For a nonstationary process, the form error is composed of two components: (1) deterministic error representing a deterministic trend surface that accounts for large-scale variation and is considered to be spatially dependent; (2) random error representing small-scale variation on the trend surface and is considered to be residuals and stochastic in nature and spatially independent. Incorporating the deterministic error into an assessment procedure is crucial in form error estimation for geometric features [12]. Numerous methods have been used to model deterministic errors. Yan and Menq [13] explored a two-step method to estimate the deterministic error. The measurements were used to construct an artificial surface and this surface was fitted to the nominal surface. Then, the deterministic error was estimated using the orthogonal deviation from the nominal surface. Furthermore, a polynomial of different orders [14], B-spline function [15], and Fourier analysis [16–18] was presented to model the systematic error. These methods required a large amount of CMM data in order to estimate the relatively large number of parameters involved in the polynomial or B-spline function approaches or to allow a clean separation of the frequencies in the Fourier analysis approach [19].

Correlation arises frequently in data observed within certain intervals of space, and the data indeed exhibits a significant amount of positive autocorrelation [20]. Measurements are often spatially correlated because they are obtained in similar machining conditions during the machining process and related to similar (local) properties of the machined material. Spatial correlation is different from temporal correlation, which is usually represented via time series models [21]. In fact, spatial correlation models allow one to represent contiguity in space rather than in time.

Sayles and Thomas [22] used structure function to model the spatial correlation in product surface quality studies. Colosimo and Semeraro [23] used a spatial autoregressive regression model (i.e., a regression model with spatial autoregression errors) to characterize the roundness of a manufactured product. Xia et al. [19] presented a Gaussian process (GP) method for modeling the deterministic errors using a Gaussian correlation function. The analysis result shows that the GP method generally gives a less biased estimate of the form error than the traditional minimum zone (MZ) and least squares (LS) methods [24–26]. Suriano et al. proposed a method for efficiently measuring and monitoring surface spatial variations by fusing multiresolution measurements and process information [27]. Furthermore, inverse distance

[1]Corresponding author.

Contributed by the Manufacturing Engineering Division of ASME for publication in the Journal of Manufacturing Science and Engineering. Manuscript received January 16, 2015; final manuscript received August 24, 2015; published online October 27, 2015. Assoc. Editor: Xiaoping Qian.

weighted interpolation (IDW) and triangulated irregular network (TIN) [28] are also widely used methods.

Little research on the spatial statistics-based methods to model deterministic errors of part form has been conducted and the literature on this topic is sparse. Spatial statistics, e.g., Kriging method, is one of most important meta-models for interpolation in random field [29,30]. Detailed descriptions of existing research on Kriging meta-modeling for interpolation are provided in a review [31]. Yang and Jackman [32] applied one univariate spatial statistic method, i.e., ordinary Kriging (OK), to predict machining part form error. The spatial correlation of the height values (Z coordinates) was modeled as an explicit function of the other two coordinates (X, Y coordinates). The general prediction method was proposed to estimate the trend of a surface component and to subtract the trend from the sample data to obtain the residuals component. The residuals were treated as stationary and a variogram was fitted to the residuals. Finally, the estimated residuals were combined with the trend surface to obtain estimates of the actual surface. The results showed that fitted surface obtained through OK can provide more accurate estimates of form error.

Yang and Jackman [32] only considered spatial correlation on height values obtained offline. With the development of the measurement equipments, more online measurement data are acquired to monitor the conditions of the machining processes. As well known, the machining conditions (cutting forces, feed rate, cutting tool vibration, etc.) are ubiquitous in machining processes and highly influence the final machining part form errors [33–35]. Chen [36] pointed out that cutting conditions, tool wear, the material properties of tool and workpiece, as well as cutting process parameters (including cutting speed, depth of cut, feed rate, tool geometry, etc.) significantly influence the form error of finished surface on machined parts. Roth et al. [37] thought a machining condition has a direct effect on part quality and proposed online sensor-based approaches for tool condition monitoring that provide a means to assess the underlying tool condition during the cutting process. Benardos and Vosniakos [38] reviewed the approaches that predict the surface form error and roughness under various machining conditions.

However, no research has combined spatial correlation with the machining conditions to analyze the surface form error for a machined part. Thus, in order to obtain a more accurate artificial surface for further improving the form error estimation, it is necessary to consider both spatial correlation on measured height values and the influence of the machining conditions. The spatial prediction for surface form error considering multiple machining conditions is a multivariate spatial estimation problem. The goal of this paper is to estimate form error using multivariate spatial statistics method.

The rest of this paper is organized as follows: the problem description is presented in Sec. 2. The method based on multivariate spatial statistics for form error estimation is developed in Sec. 3, which considers both spatial correlation of height value measurements and the influence of the machining conditions. And an illustrated example is presented. In Sec. 4, the simulation experiment and performance analysis are conducted on univariate and multivariate spatial statistics methods. In Sec. 5, two case studies are presented to validate the developed method based on the actual data. Finally, the conclusions are given in Sec. 6.

2 Problem Description and Univariate Spatial Method for Form Error Estimation

A set of points measured on the part surface can be denoted by

$$\{Z(s), s \in D\} \tag{1}$$

where s is a spatial location vector in R^2 on the surface, and the index set D defines a finite region on the surface.

Through a CMM, a set of height value measurements, $\{z(s_1), \ldots, z(s_n)\}$, can be collected from locations $\{s_1, \ldots, s_n\}$ located within this finite region D. Traditionally, the collected points $\{z(s_1), \ldots, z(s_n)\}$ are directly used to estimate surface form error with LS or MZ methods (see Fig. 1(*a*), unit: mm). More accurate form can be characterized by directly obtaining more data from the manufactured surface. However, collecting a large number of measured points requires high cost and decreases production efficiency. Univariate spatial statistics (e.g., Kriging) make it possible to interpolate some points and to reconstruct artificial surfaces for form error estimation. Univariate spatial statistics method outperforms the direct method in some cases [39] (see Fig. 1(*b*)).

Univariate spatial statistics method supposes that the height values on the surface $\{Z(s), s \in D\}$ are real-valued intrinsically stationary random fields, which for all $s, h \in R$ satisfies [40]

$$E[Z(s) - Z(s+h)] = 0 \tag{2}$$

$$2\gamma(h) = \mathrm{Var}[Z(s) - Z(s+h)] = E[Z(s) - Z(s+h)]^2 \tag{3}$$

where $E(\cdot)$ is the mathematic expectation and $\mathrm{Var}(\cdot)$ is the variance of the increment between two points on the surface with the distance h, $2\gamma(h)$ called variogram in spatial statistics, denotes the degree of spatial correlation in a spatial stationary process. In addition, the correlation at various locations depends only on the distance of two locations $h = \|s_i - s_j\|$.

The semivariogram (called variogram for short) $\gamma(h)$ is a measurement for the spatial correlation structure at a given distance h, which is denoted by [41]

$$\hat{\gamma}(h) = \frac{1}{2N_n(h)} \sum_{i,j \in N_n(h)} [Z(s_i) - Z(s_j)]^2,\ h \in R \tag{4}$$

where n is the total number of measured points, $N_n(h) = \{(i,j): i,j \in [1,n], \|s_i - s_j\| = h\}$ is the number of pairs of measurements with the given distance h, s_i, and s_j are the locations of the measured points. The summation is conducted over all i, j pairs in the distance class.

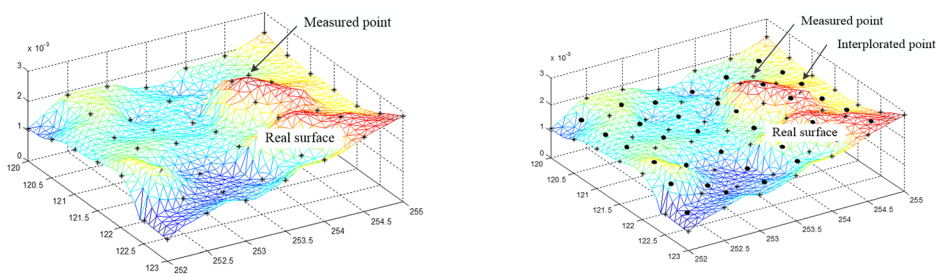

(*a*) (*b*)

Fig. 1 Methods of form error estimation: (*a*) by directly measured points and (*b*) by interpolated and measured points

When n surface data points, $\{z(s_1), z(s_2), \ldots, z(s_n)\}$, are measured, the height value $Z(s_0)$ at a new point location s_0 can be estimated through Kriging with the help of variogram. In particular, Kriging estimation $Z(s_0)$ is determined by a linear combination of the data values $Z^*(s_0) = \sum_{i=1}^{n} \lambda_i [Z(s_i)]$ where λ_i are weights chosen on the condition that the estimation is unbiased and the estimation error variance is smallest.

OK uses sparse scatting measured points to interpolate more certain points on the part surface and to reconstruct a more accurate artificial surface for form error estimation, which excels the form error estimation only with the limited direct measurements.

However, the height values of some interpolated points are not exactly equal to that on the real surface (see Fig. 2, unit: mm). There is a deviation e between the estimation and the real surface height value, which leads to the inaccuracy artificial surface construction and form error estimation. The reason of this phenomenon is that Kriging predicting the height values only uses known height value information on measured locations considering the spatial correlation. It may not meet the accuracy demand of form error estimation based on univariate spatial correlation. How to decrease this deviation e to improve the precision of form error estimation is one of the crucial problems.

In fact, the form error estimation of a part surface is greatly influenced by the machining conditions, such as the cutting forces, feed rate, and tool vibration. To establish a more accurate artificial surface, it is necessary to combine spatial correlation both on the height values and on the machining conditions.

3 The Proposed Multivariate Spatial Statistics Method for Form Error Estimation

3.1 Variogram and Cross-Variogram. Usually, the real values of the machining conditions at different locations can be online obtained by sensors. The values of the machining conditions are denoted by

$$\{V_t(s), s \in D\} \tag{5}$$

where s is a spatial location vector in the finite region D on the surface and t is the index of the machining condition types.

Incorporated with the machining conditions V_t, the spatial correlation takes place in the process of $\{Z(s), s \in D\}$ and $\{V_t(s), s \in D\}$. Therefore, the variogram has to be extended to cross-variogram, which characterizes the multivariate spatial correlation

$$2\gamma_{AB}(h) = \mathrm{Var}[A(s) - B(s+h)] = E[A(s) - B(s+h)]^2 \tag{6}$$

The sample cross-variogram by n measured points conducted from autovariogram is calculated as

$$\hat{\gamma}_{AB}(h) = \frac{1}{2N_n^{AB}(h)} \sum_{i,j \in N_n^{AB}(h)} [A(s_i) - A(s_j)][B(s_i) - B(s_j)], \quad \times h \in R^d, A, B \in \{Z, V_t\} \tag{7}$$

where $N_n^{AB}(h) = \{(i,j) : i,j \in [1,n], \|s_i - s_j\| = h\}$ is the number of pairs of measurements of the first variable A and the second variable B at locations s_i and s_j when the distance between s_i and s_j fits a distance class h. The summation is conducted over all i, j pairs in the distance class.

The proof of Eq. (7) is provided in the Appendix. For more details on how to construct cross-variogram from autovariogram, refer to Ref. [42]. Cross-variogram values can increase or decrease with distance h depending on the correlation between variable A and variable B. When models are fitted to the variogram and cross-variogram, the Cauchy–Schwartz relation must be checked to guarantee a correct estimation variance [43,44]

$$|\gamma_{AB}(h)| \le |\gamma_{AA}(h)^* \gamma_{BB}(h)|^{\frac{1}{2}}, A, B \in \{Z, V_t\} \tag{8}$$

The Cauchy–Schwarz inequality is considered in the variogram modeling process to avoid facing with negative definite matrices and insoluble equation system in CK algorithm [45]. Therefore, the Cauchy–Schwartz inequality should be satisfied whether using the cross-covariances or using the cross-variograms [46]. Many efforts on constructing valid cross-covariance structure in multivariate spatial process can be found in the literature of design and analysis of computer experiments, where a covariance representation (instead of variogram) of the Kriging method is often used [47–50]. It can be shown that the Cauchy–Schwartz inequality is necessary but not sufficient for joint non-negative definiteness of the fitted cross-covariance models. There is a controversy over the applicability of the Cauchy–Schwartz inequality to the cross-variogram matrices [51]. In order to generate non-negative definite functions for cross-variogram, Rehmanand Shapiro [52] and Armstrong and Diamond [53] proposed the Fourier transform to follow the result which is a natural generalization of the "sufficient" part of Bochner's theorem.

Cross-variogram $\gamma_{AB}(h)$, as well as variogram $\gamma(h)$, can be modeled to a theoretical variogram through a least square fitting process. As the distance h gets larger, the variogram values increase, which indicates that as two locations get farther apart, the expected difference of the measured values between these two locations increases as well.

The theoretical variogram model has three main parameters: (1) Nugget (C_0) is the semivariance at zero distance due to measurement error and microscale variation. (2) Sill ($C_0 + C_1$) is the semivariance value of the plateau, which is the maximum height of the variogram curve. As distance h gets large, the correlation between the two points becomes negligible and the value of variogram tends to be stationary. (3) Correlation length (a) is the distance at which the semivariance achieves the plateau, which means that pairs of points larger than this distance apart are negligibly correlated.

There exist various models for fitting diverse empirical variograms in practice. Some popular theoretical fitting models include

$$\text{Spherical model}: \ \gamma(h) = \begin{cases} C_0 + C_1 \left[1.5\left(\frac{h}{a}\right) - 0.5\left(\frac{h}{a}\right)^3\right], 0 \le h \le a \\ C_0 + C_1, h > a \end{cases} \tag{9}$$

$$\text{Exponential model}: \ \gamma(h) = C_0 + C_1\left[1 - \exp\left(-\frac{3h}{a}\right)\right] \tag{10}$$

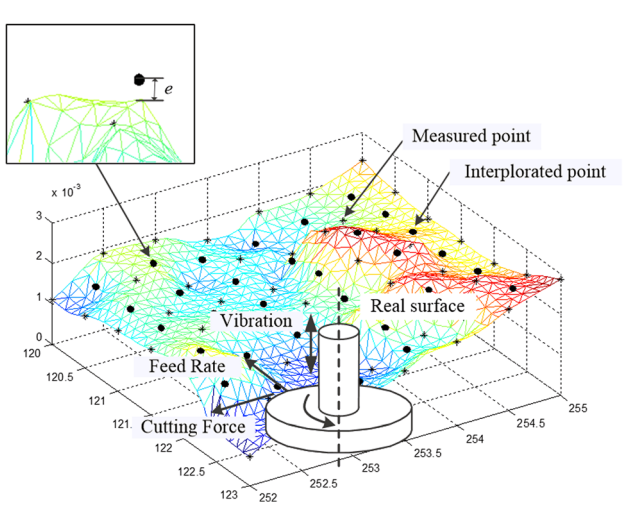

Fig. 2 Influence of machining conditions

$$\text{Periodicity model}:\ \gamma(h) = W\left\{1 - \frac{1}{\theta}\sin(\theta)\right\}, \theta = \frac{2\pi h}{\omega} \quad (11)$$

where W is the amplitude and ω is the wavelength of periodicity variogram.

The differences among the theoretical variogram models vary in the fitting degree, thus it is important to choose the best theoretical variogram model by appropriate fitting standards. Among them, the ratio of the structural effects is frequently used, which is the ratio of nugget to sill and sill $(C_1/C_0 + C_1)$. It characterizes the degree of spatial heterogeneity, which means the spatial variability caused by the autocorrelation occupies the proportion of the total variation of the system. The larger the ratio is, the stronger the spatial correlation is. The stronger spatial correlation for the theoretical variogram, the more precise estimation for the predictive modeling interpolation by spatial statistics method, and thus it makes form error estimation more accurate.

3.2 Multivariate Spatial Method. CK is a multivariate spatial interpolation method based on the multivariate spatial correlation structure [54]. Compared to Kriging, it organizes not only a sparse set of data (height value, denoted Z) but also other data sets that are dense and can be sampled more frequently and regularly (machining condition, denoted V_t). Figure 3 shows the different variables and data information used in Kriging and CK to interpolate the unmeasured points. CK requires more information which is designated by machining conditions V_1, V_2. In Fig. 3, black dots $Z(s_i), i \in \{1,2,3,4\}$ are measurements of height values at locations s_i, and black squares are unmeasured points s_0 that will be interpolated. $V_1(s_a), a \in \{2,3,4,6,7\}$ and $V_2(s_b), b \in \{1,2,4,5,6\}$ are measurements of machining conditions at locations s_a and s_b, locations s_5, s_6, s_7 on surface in Fig. 3(*b*) are new measured points required for CK.

The height value Z is the target variable and the machining condition V_t gives the supportive information for the target variables. Both autocorrelation and cross-correlation between Z and all other machining condition variable V_t are used to make better predictions. In fact, at some location s*, if there is only the measurement of machining condition variable V_t (as the measurement $A(s^*)$),and there is not any measurement of height value Z (as the measurement $B(s^*)$), the data of $A(s^*)$ is still useful for the estimator. Even if there is no cross-correlation between Z and V_t, or even if no measurement of Z at some locations, it can still fall back on the autocorrelation for height value. So CK can theoretically do no worse than Kriging. At the same time, the deviation between the real surface and the estimated height value in the univariate spatial method can more or less decrease. Therefore, it is possible to improve the precision of form error estimation using CK.

Incorporated with machining conditions, the height value $Z(s_0)$ at the unmeasured point location s_0 can also be determined by a linear combination of the measured CMM data. The interpolated height value by CK can be calculated by [55,56]

$$Z^*_{\mathrm{CK}}(s_0) = \sum_{i_1=1}^{N_1} \lambda_{1i_1} V_1(s_{1i_1}) + \sum_{i_2=1}^{N_2} \lambda_{2i_2} V_2(s_{2i_2}) + \cdots + \sum_{i_T=1}^{N_T} \lambda_{Ti_T} V_T(s_{Ti_T}) + \sum_{k=1}^{N_0} \lambda_{0k} Z(s_{0k}) \quad (12)$$

where $V_t(t = 1,2,\ldots,T)$ are T machining conditions, and Z is the main variable, height value, on measured points. $s_{ti_t}(t = 1,\ldots,T)$ are measured locations of T machining conditions, and s_{0k} is the measured location of height value. $N_t(t = 1,2,\ldots,T)$ are the total numbers of the measured locations for T machining conditions, and N_0 is the total number of measured locations for height value. $\lambda_{ti_t}(t = 1,\ldots,T)$ are weights characterized by the impacts of machining conditions on the height value of the estimated point s_0, and λ_{0k} characterizes the impact of the height values from known measured locations.

Since CK weights have to satisfy the unbiased constraint $E[Z^*_{\mathrm{CK}}(s_0) - Z(s_0)] = 0$, calculated by

$$\begin{aligned} &E[Z^*_{\mathrm{CK}}(s_0) - Z(s_0)] \\ &= E\{[\sum_{i_1=1}^{N_1}\lambda_{1i_1}V_1(s_{1i_1}) + \sum_{i_2=1}^{N_2}\lambda_{2i_2}V_2(s_{2i_2}) + \cdots \\ &+ \sum_{i_T=1}^{N_T}\lambda_{Ti_T}V_T(s_{Ti_T}) + \sum_{k=1}^{N_0}\lambda_{0k}Z(s_{0k})] - Z(s_0)\} \\ &= E\{Z(s_0)\}[\sum_{k=1}^{N_0}\lambda_{0k} - 1] + E\{V_1(s_{1i_1})\}\sum_{i_1=1}^{N_1}\lambda_{1i_1} \\ &+ E\{V_2(s_{2i_2})\}\sum_{i_2=1}^{N_2}\lambda_{2i_2} + \cdots + E\{V_T(s_{Ti_T})\}\sum_{i_T=1}^{N_T}\lambda_{Ti_T} = 0 \end{aligned} \quad (13)$$

Then obtain

$$\sum_{k=1}^{N_0}\lambda_{0k} = 1, \quad \sum_{i_1=1}^{N_1}\lambda_{1i_1} = 0, \quad \sum_{i_2=1}^{N_2}\lambda_{2i_2} = 0 \quad ,\ldots, \quad \sum_{i_T=1}^{N_T}\lambda_{Ti_T} = 0 \quad (14)$$

Minimizing CK error variance $\mathrm{Var}[Z^*_{\mathrm{CK}}(s_0) - Z(s_0)]$, calculated by

$$\begin{aligned} &\min\{\mathrm{Var}[Z_{\mathrm{CK}}{}^*(s_0) - Z(s_0)]\} \\ &= E\{\{[Z_{\mathrm{CK}}{}^*(s_0) - Z(s_0)] - E[Z_{\mathrm{CK}}{}^*(s_0)] - Z(s_0)\}^2\} \\ &= E\{[Z_{\mathrm{CK}}{}^*(s_0) - Z(s_0)]^2\} \\ &= E\Big\{\Big\{\Big[\sum_{i_1=1}^{N_1}\lambda_{1i_1}V_1(s_{1i_1}) + \sum_{i_2=1}^{N_2}\lambda_{2i_2}V_2(s_{2i_2}) + \cdots \\ &+ \sum_{i_T=1}^{N_T}\lambda_{Ti_T}V_T(s_{Ti_T}) + \sum_{k=1}^{N_0}\lambda_{0k}Z(s_{0k})\Big] - Z(x_0)\Big\}^2\Big\} \end{aligned} \quad (15)$$

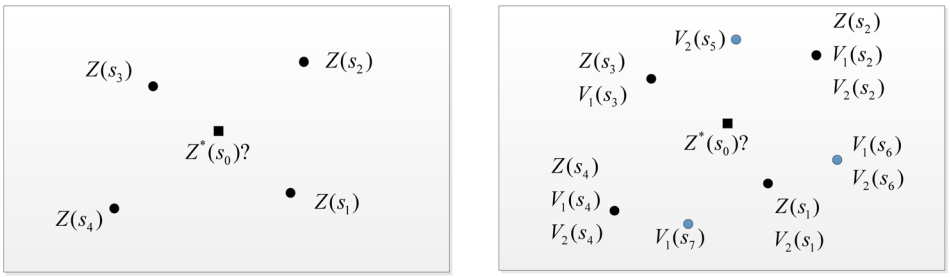

(*a*) (*b*)

Fig. 3 Comparison of Kriging and CK variables: (*a*) Kriging and (*b*) CK

Lagrange multipliers are usually used to adjoin constraint equation (15) to an objective function. CK error variance is minimized. Then obtain

$$\begin{cases} \sum_{i_1=1}^{N_1}\lambda_{1i_1}\gamma_{11}(s_{1i}-s_{I_1})+\sum_{i_2=1}^{N_2}\lambda_{2i_2}\gamma_{12}(s_{2i_2}-s_{I_2})+\cdots+\sum_{i_T=1}^{N_T}\lambda_{Ti_T}\gamma_{1T}(s_{Ti_T}-s_{I_T})+\sum_{k=1}^{N_0}\lambda_{0k}\gamma_{10}(s_{0k}-s_K)+\mu_1=\gamma_{10}(s_0-s_{I_1}) \\ \sum_{i_1=1}^{N_1}\lambda_{1i_1}\gamma_{21}(s_{1i}-s_{I_1})+\sum_{i_2=1}^{N_2}\lambda_{2i_2}\gamma_{22}(s_{2i_2}-s_{I_2})+\cdots+\sum_{i_T=1}^{N_T}\lambda_{Ti_T}\gamma_{2T}(s_{Ti_T}-s_{I_T})+\sum_{k=1}^{N_0}\lambda_{0k}\gamma_{20}(s_{0k}-s_K)+\mu_2=\gamma_{20}(s_0-s_{I_2}) \\ \cdots \\ \sum_{i_1=1}^{N_1}\lambda_{1i_1}\gamma_{T1}(s_{1i}-s_{I_1})+\sum_{i_2=1}^{N_2}\lambda_{2i_2}\gamma_{T2}(s_{2i_2}-s_{I_2})+\cdots+\sum_{i_T=1}^{N_T}\lambda_{Ti_T}\gamma_{TT}(s_{Ti_T}-s_{I_T})+\sum_{k=1}^{N_0}\lambda_{0k}\gamma_{t0}(s_{0k}-s_K)+\mu_T=\gamma_{T0}(s_0-s_{I_T}) \\ \sum_{i_1=1}^{N_1}\lambda_{1i_1}\gamma_{01}(s_{1i}-s_{I_1})+\sum_{i_2=1}^{N_2}\lambda_{2i_2}\gamma_{02}(s_{2i_2}-s_{I_2})+\cdots+\sum_{i_T=1}^{N_T}\lambda_{Ti_T}\gamma_{0T}(s_{Ti_T}-s_{I_T})+\sum_{k=1}^{N_0}\lambda_{0k}\gamma_{00}(s_{0k}-s_K)+\mu_0=\gamma_{00}(s_0-s_K) \end{cases} \tag{16}$$

where the addition parameters $\mu_i, i = 0, 1, 2, \ldots, T$ are Lagrange multipliers used in minimization of CK error variance $\sigma_{\mathrm{CK}}{}^2$ to satisfy the unbiased condition, and $\gamma_{pq}(s_i - s_j)$, $p, q = 0, 1, 2, \ldots, T$ is the cross-variogram $(p \neq q)$ or autovariogram $(p = q)$ value $\gamma_{pq}(h)$ between the height values and machining conditions for the distance $h = \|s_i - s_j\|$ calculated in spatial correlation.

CK weights can be calculated by the two constraints (Eqs. (14) and (16)). Combined the interpolated points with the measured points, the artificial surface can be reconstructed closer to the real surface, which makes it more precise for form error estimation.

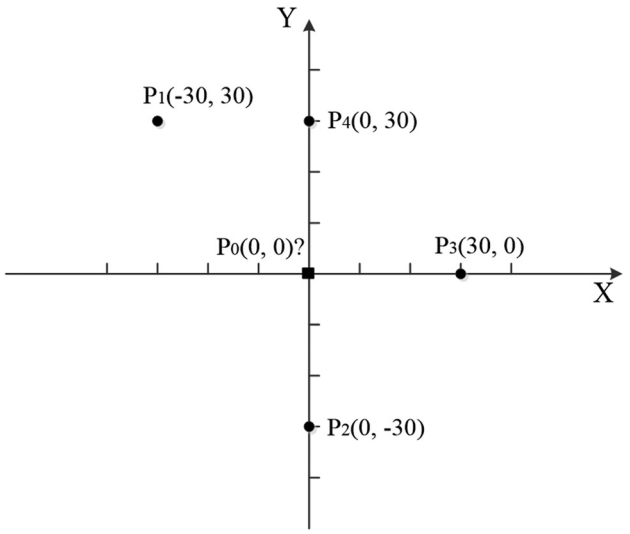

Fig. 4 Distribution of measured and estimated points

3.3 An Illustrated Example. In order to illustrate the proposed multivariate spatial method, a sample surface in the 30×30 square with four measured points $P_1(-30, 30), P_2(0, -30), P_3(30, 0), P_4(0, 30)$ is presented (see Fig. 4).

At each point, there are three variables (two independent machining conditions V_1, V_2 and one dependent height value Z) that have the spatial correlations. The machining condition V_1 at point P_1, P_2, P_3, P_4 is known as $V_{11} = 8, V_{12} = 3, V_{13} = 10, V_{14} = 7$, the machining condition V_2 at point P_1, P_2 is known as $V_{21} = 4, V_{22} = 11$, and the height value Z at point P_1, P_2 is known as $Z_1 = 9, Z_2 = 12$. The goal is to estimate the value of the variable Z at point $P_0(0, 0)$. The autovariogram of the variables V_1, V_2, Z is calculated as (exponential model)

$$\gamma_{11}(h) = 0.06 + 0.7(1 - \exp(-h/300))(V_1)$$
$$\gamma_{22}(h) = 0.14 + 0.8(1 - \exp(-h/200))(V_2)$$
$$\gamma_{00}(h) = 0.22 + 0.9(1 - \exp(-h/100))(Z)$$

The cross-variogram between variables is calculated by spherical model as

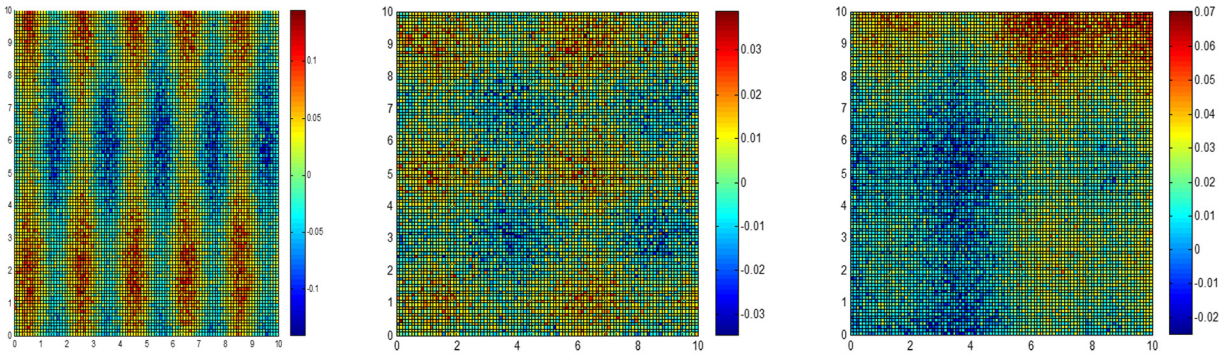

(*a*) (*b*) (*c*)

Fig. 5 Color-coded images of simulated surfaces: (*a*) Case1, (*b*) Case 2, and (*c*) Case 3

$$\gamma_{12}{}^{+}(h) = \gamma_{20}{}^{+}(h) = \gamma_{10}{}^{+}(h) = \begin{cases} 0.4 + 0.32(1.5(h/100) - 0.5(h/100)^3), h \le 100 \\ 0.72, h > 100 \end{cases}$$

$$\gamma_{12}(h) = 0.5[\gamma_{12}{}^{+}(h) - \gamma_{11}(h) - \gamma_{22}(h)]$$

$$\gamma_{20}(h) = 0.5[\gamma_{20}{}^{+}(h) - \gamma_{22}(h) - \gamma_{00}(h)]$$

$$\gamma_{10}(h) = 0.5[\gamma_{10}{}^{+}(h) - \gamma_{11}(h) - \gamma_{00}(h)]$$

According to Eqs. (14)–(16), the constraints are given by

$$\sum_{k=1}^{N_0}\lambda_{0k} = 1, \sum_{i=1}^{N_1}\lambda_{1i} = 0, \sum_{j=1}^{N_2}\lambda_{2j} = 0, \ (N_1 = 4, \quad N_2 = 2, \quad N_0 = 2)$$

$$\sum_{i-1}^{N_1}\lambda_{1i}\gamma_{11}(s_{1i} - s_I) + \sum_{j-1}^{N_2}\lambda_{2j}\gamma_{12}(s_{2j} - s_J) + \sum_{k-1}^{N_0}\lambda_{0k}\gamma_{10}(s_{0k} - s_K) + \mu_1 = \gamma_{10}(s_0 - s_I)$$

$$\sum_{i-1}^{N_1}\lambda_{1i}\gamma_{21}(s_{1i} - s_I) + \sum_{j-1}^{N_2}\lambda_{2j}\gamma_{22}(s_{2j} - s_J) + \sum_{k-1}^{N_0}\lambda_{0k}\gamma_{20}(s_{0k} - s_K) + \mu_2 = \gamma_{20}(s_0 - s_J)$$

$$\sum_{i-1}^{N_1}\lambda_{1i}\gamma_{01}(s_{1i} - s_I) + \sum_{j-1}^{N_2}\lambda_{2j}\gamma_{02}(s_{2j} - s_J) + \sum_{k-1}^{N_0}\lambda_{0k}\gamma_{00}(s_{0k} - s_K) + \mu_0 = \gamma_{00}(s_0 - s_K)$$

Convert the constraints to the matrix, and the weights are achieved by

$$\begin{bmatrix} \lambda_{11} \\ \lambda_{12} \\ \lambda_{13} \\ \lambda_{14} \\ \lambda_{21} \\ \lambda_{22} \\ \lambda_{01} \\ \lambda_{02} \\ \mu_1 \\ \mu_2 \\ \mu_0 \end{bmatrix} = \begin{bmatrix} 0.0600 & 0.2003 & 0.2003 & 0.1266 & 0.1000 & 0.0527 & 0.0600 & -0.0932 & 1 & 0 & 0 \\ 0.2003 & 0.0600 & 0.1523 & 0.1896 & 0.0527 & 0.1000 & -0.0932 & 0.0600 & 1 & 0 & 0 \\ 0.2003 & 0.1523 & 0.0600 & 0.1523 & 0.0527 & 0.0731 & -0.0932 & -0.0460 & 1 & 0 & 0 \\ 0.1266 & 0.1869 & 0.1523 & 0.0600 & 0.0808 & 0.0596 & -0.0201 & -0.0798 & 1 & 0 & 0 \\ 0.1000 & 0.0527 & 0.0527 & 0.0808 & 0.1400 & 0.3680 & 0.0200 & -0.1771 & 0 & 1 & 0 \\ 0.0527 & 0.1000 & 0.0731 & 0.0596 & 0.3680 & 0.1400 & -0.1771 & 0.0200 & 0 & 1 & 0 \\ 0.0600 & -0.0932 & -0.0932 & -0.0201 & 0.0200 & -0.1771 & 0.2200 & 0.6598 & 0 & 0 & 1 \\ -0.0932 & 0.0600 & -0.0460 & -0.0798 & -0.1771 & 0.0200 & 0.6598 & 0.2200 & 0 & 0 & 1 \\ 1 & 1 & 1 & 1 & 0 & 0 & 0 & 0 & 0 & 0 & 0 \\ 0 & 0 & 0 & 0 & 1 & 1 & 0 & 0 & 0 & 0 & 0 \\ 0 & 0 & 0 & 0 & 0 & 0 & 1 & 1 & 0 & 0 & 0 \end{bmatrix}^{-1} \times \begin{bmatrix} -0.046 \\ -0.0201 \\ -0.0201 \\ -0.0201 \\ -0.1163 \\ -0.0825 \\ 0.5312 \\ 0.4533 \\ 0 \\ 0 \\ 1 \end{bmatrix}$$

Through the MATLAB programming procedure, the values of the weights are obtained

$$\lambda_{11} = 0.3703; \ \lambda_{12} = 0.2212; \ \lambda_{13} = -0.2783$$

$$\lambda_{14} = -0.3132; \ \sum \lambda_{1i} = 0$$

$$\lambda_{21} = 0.0456; \ \lambda_{22} = -0.0456; \ \sum \lambda_{2j} = 0$$

$$\lambda_{31} = 0.4515; \ \lambda_{32} = 0.5485; \ \sum \lambda_{0k} = 1$$

$$\mu_1 = 0.0047; \ \mu_2 = -0.0266; \ \mu_0 = 0.0271$$

The estimated height value on $P_0(0,0)$ using CK can be obtained

$$Z^*_{\mathrm{CK}}(0,0) = \sum_{i=1}^{N_1}\lambda_{1i}V_1(s_{1i}) + \sum_{j=1}^{N_2}\lambda_{2j}V_2(s_{2j}) + \sum_{k=1}^{N_0}\lambda_{0k}Z(s_{0k})$$

$$= 8.9773$$

The height value of the unmeasured point $P_0(0,0)$ can be achieved by CK using the machining conditions. The cross-variogram function is simply calculated by known autovariogram, and all these variograms characterize the spatial correlation on this exampled surface.

Table 1 Manufacturing scenarios for form error estimation

Scenarios		L	R	A_x	A_y	λ_x	λ_y	$A_{\mathrm{vib}x}$	$A_{\mathrm{vib}y}$	$\lambda_{\mathrm{vib}x}$	$\lambda_{\mathrm{vib}y}$	σ_ε
Case 1	OK	20	0.015	0.05	0.03	2	8	—	—	—	—	0.02
	CK	20	0.015	0.05	0.03	2	8	0.025	0.015	1	4	0.02
Case 2	OK	20	0.025	0.006	0.007	5	4	—	—	—	—	0.008
	CK	20	0.025	0.006	0.007	5	4	0.003	0.0035	2.5	2	0.008
Case 3	OK	20	0.25	0.008	0.008	5	8	—	—	—	—	0.008
	CK	20	0.25	0.008	0.008	5	8	0.004	0.004	2.5	4	0.008

4 Comparison of Univariate and Multivariate Spatial Statistics Methods Using Simulated Data

4.1 Simulation Comparison Procedure. In order to compare CK considering machining conditions with OK without considering machining conditions for form error estimation, the simulation experiment has been conducted. Below is the simulation procedure

Step 1: Simulate a geometric feature on the surface with an area of $10 \times 10\ \text{mm}^2$.

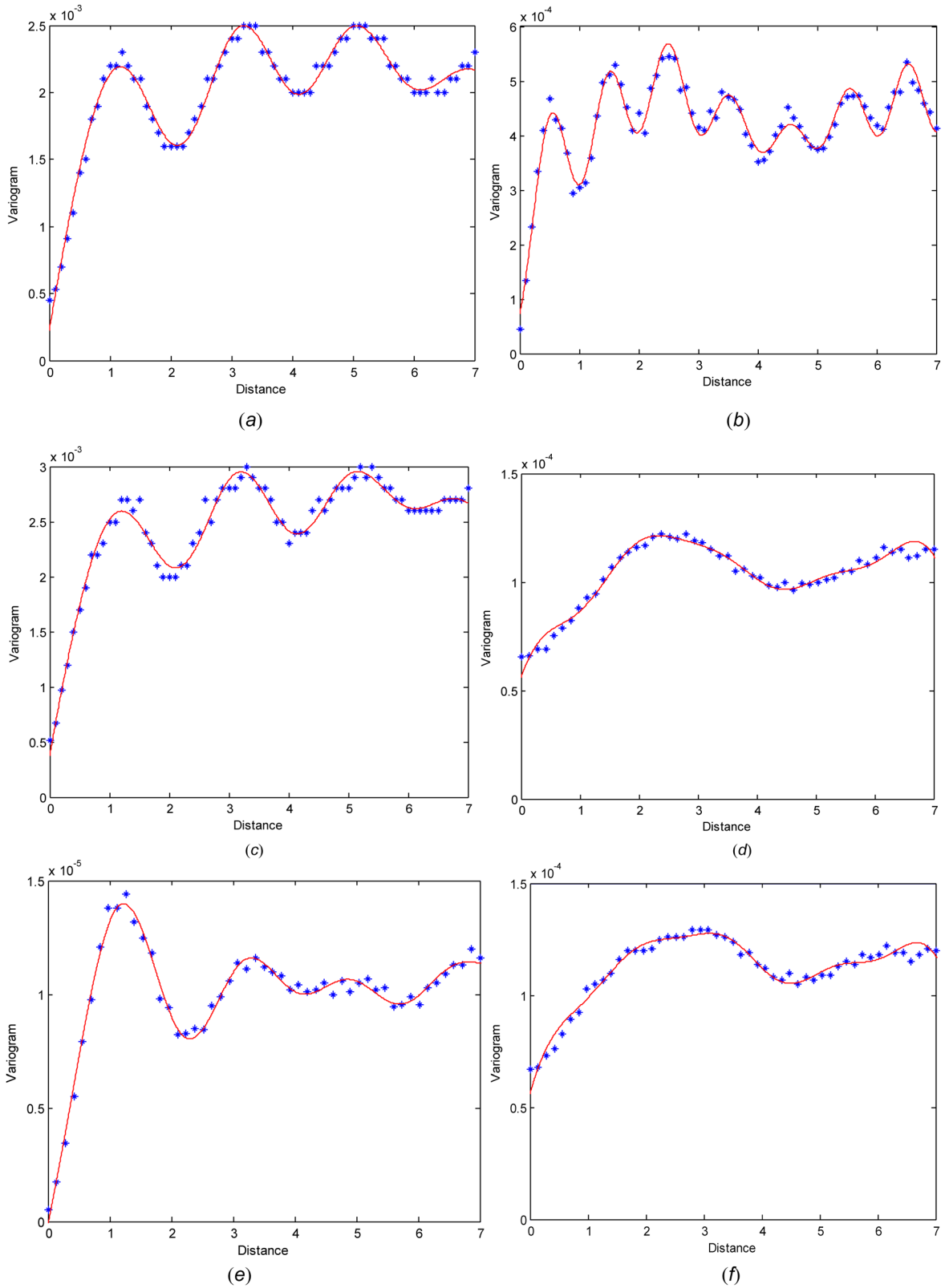

Fig. 6 Theoretical variogram of height and vibration and cross-variogram. (*a*) Case 1: height value, (*b*) case 1: vibration, (*c*) case 1: cross-variogram of height value and vibration, (*d*) case 2: height value, (*e*) case 2: vibration, (*f*) case 2: cross-variogram of height value and vibration, (*g*) case 3: height value, (*h*) case 3: vibration, and (*i*) case 3: cross-variogram of height value and vibration.

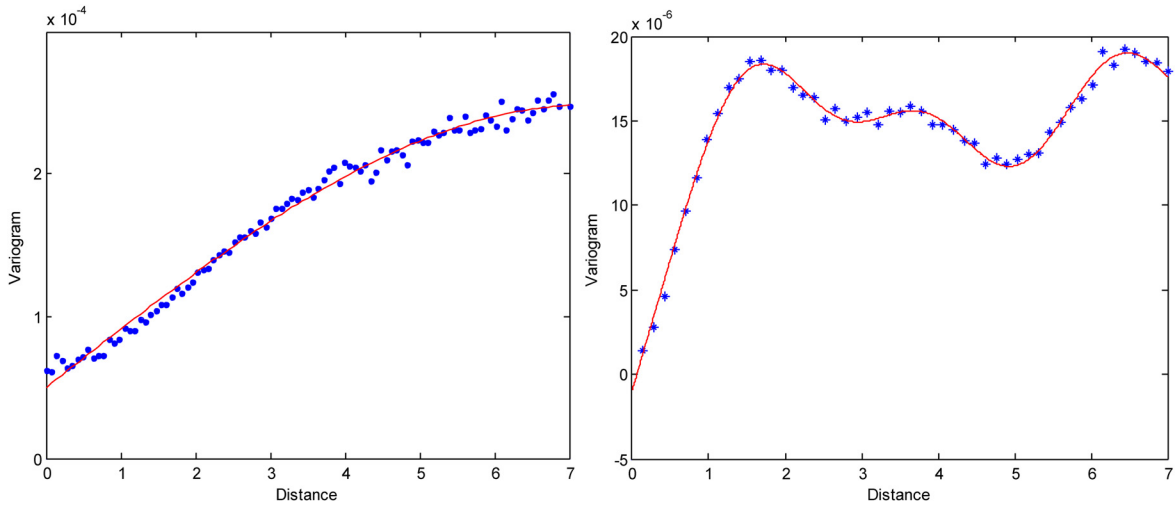

(*g*)

(*h*)

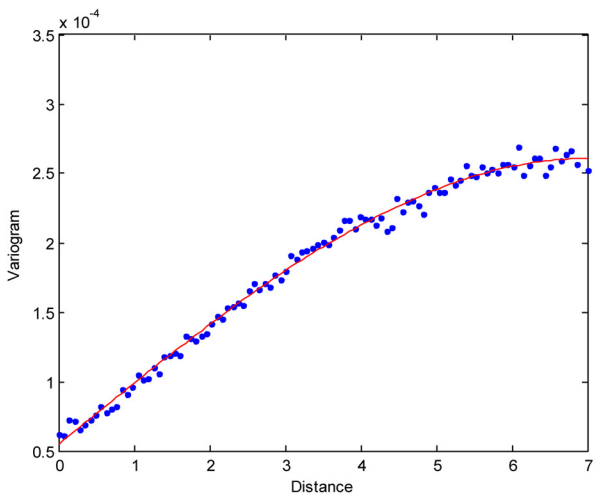

(*i*)

Fig. 6 (Continued)

Step 2: Generate a dense enough set of measurements every 0.1 mm, a total of $N = 10{,}000$ points on the selected geometric feature so that the measurements closely represent the actual surface. In an OK simulation, only the height values are generated; while in CK simulation, the height values and one of the machining conditions—machine tool vibration value—are generated at the same time corresponding to locations.

Step 3: Select $M = 1000$ data points from the set of dense measurements. The M locations and their corresponding observations are chosen using a random sampling approach. This method enforces M samples that are evenly spread over the surface.

Step 4: Calculate the variogram for the height, vibration value, and the cross-variogram between the height and the vibration using M selected sample data points.

Step 5: Take (M–m) locations as samples to estimate the height value of $m = 50$, 100, 150, 200, 250, 300, which are as training samples using OK. Randomly remove half of the M height values, but insert their corresponding vibration value, and then take (M–m) locations as testing samples to estimate the height value of m training samples using CK.

Step 6: For $m = 50$, 100, 150, 200, 250, 300, the height value estimations determine the flatness error and denoted by f_{CK} (mm) when using CK, and by f_{OK} (mm) when using OK. Determine the form error f^* (mm) from the real height value using the individual points and treat it as the "true" flatness error.

Step 7: Calculate the form error estimation assessment ratios, f_{CK}/f^* and f_{OK}/f^*. A ratio closer to one indicates a less biased estimation.

Step 8: Repeat steps (5)–(7) 50 times for each m and generate a box–whisker plot of the flatness error estimation assessment.

In this simulation, flatness feature is simulated. The data points from the part surface are generated by the following function modified from Dowling's one-dimension function for straight feature [39]:

$$z(x,y) = \frac{64}{L^6}R\left(x^3(L-x)^2\right) + \frac{64}{L^6}R\left(y^3(L-y)^2\right) + A_x \sin\left(\frac{2\pi}{\lambda_x}x\right) + A_y \sin\left(\frac{2\pi}{\lambda_y}y\right) + \varepsilon \tag{17}$$

$$\text{vibraion}\ (x,y) = A_{\text{vibx}} \sin\left(\frac{2\pi}{\lambda_{\text{vibx}}}x\right) + A_{\text{viby}} \sin\left(\frac{2\pi}{\lambda_{\text{viby}}}y\right) \tag{18}$$

where the first two terms of Eq. (17) represent the surface deflection, the third and fourth terms are wave patterns and the last one

is the random error, assumed to be $N(0, \sigma_\varepsilon^2)$. L is the length of the straight feature, A is the sine wave amplitude ($A_x, A_y, A_{\text{vibx}}, A_{\text{viby}}$, respectively, represent the sine wave amplitude of height value and vibration value in direction of x-axis and y-axis), λ is the wavelength ($\lambda_x, \lambda_y, \lambda_{\text{vibx}}, \lambda_{\text{viby}}$, respectively, represent the sine wavelength of height value and vibration value in direction of X-axis and Y-axis), and R is the deflection range.

Table 1 shows the parameters in simulated machining scenarios for form error estimation. The simulated surfaces images for different cases are shown in Fig. 5.

4.2 Simulation Results and Discussion. The fitting theoretical variograms of the height and vibration and their cross-variograms for different cases in step 4 in Sec. 4.1. are shown in

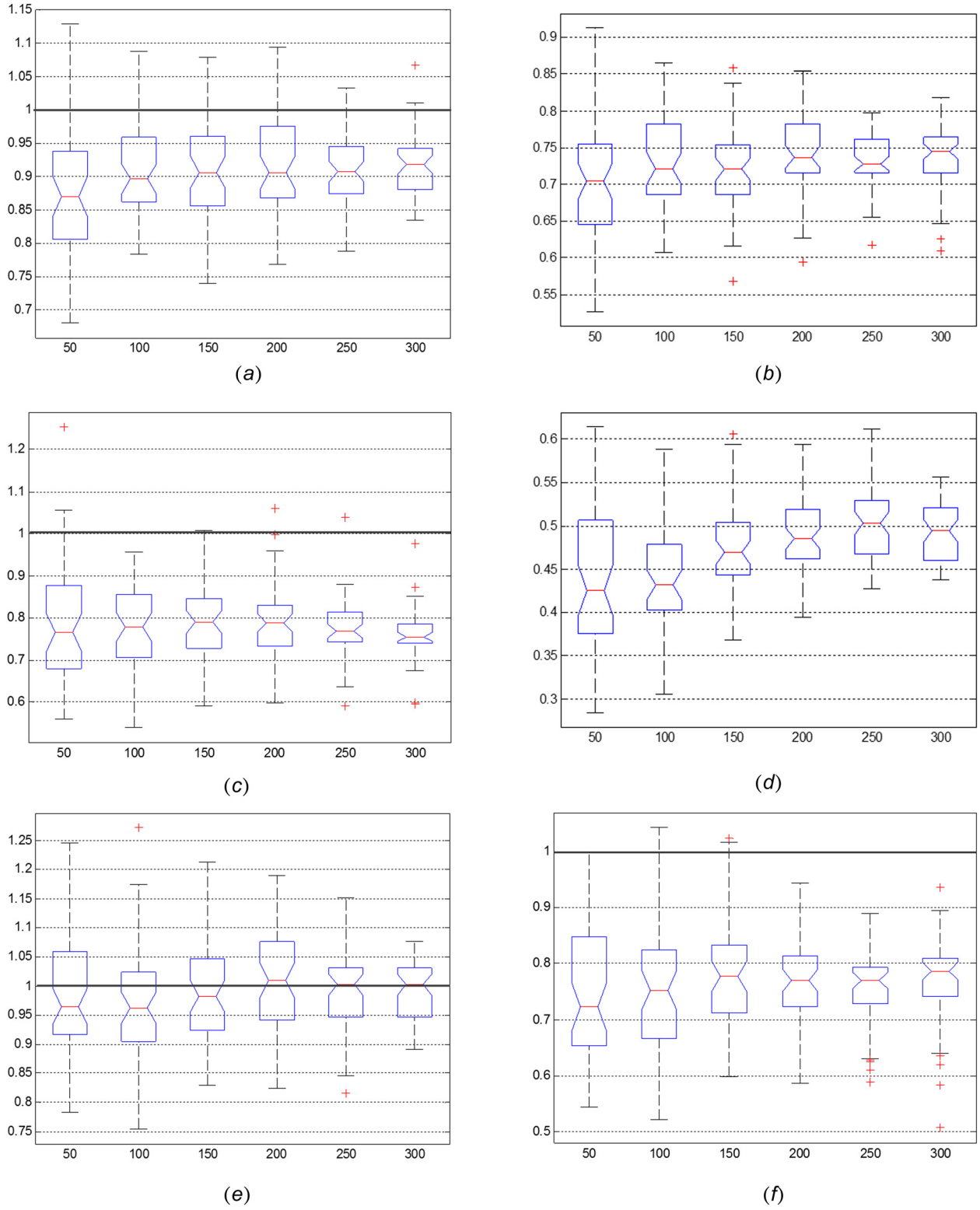

Fig. 7 Box–whisker plot of flatness error estimation comparison for different cases. (*a*) Case 1: CK, (*b*) case 1: OK, (*c*) case 2: CK, (*d*) case 2: OK, (*e*) case 3: CK, and (*f*) case 3: OK.

Fig. 8 Engine cylinder blocks processed by a major domestic car manufacturer

Fig. 6. The height variograms and cross-variograms for case 3 are modeled by spherical models, and the rest are fitted by periodicity models.

Figure 7 shows the ratios of form error estimation for flatness feature. In each box–whisker plot, the locations of the upper limit, the 75% quantile, the median, the 25% quantile, and the lower limit are shown. The crosses outside of the upper and lower limits are usually considered as outliers. The solid line indicates that the estimation of flatness error is the same as the true flatness error (i.e., estimated ratio is equal to one). In other words, the best method is the one that consistently produces box–whisker plots closest to the solid line. From Fig. 7, some findings are obtained

(1) The proposed CK based method performs significantly better than OK when systematic machining errors exist. For instance, in Case 1 the flatness error estimation assessment ratio is between 0.7 and 0.75 for OK while between 0.85 and 0.95 for CK.
(2) By comparison, OK tends to underestimate the flatness error, even when using a relatively large sample size. The reason is that the flatness error estimation assessment benefits from CK's ability to capture the systematic machining errors like the influence of vibration on height value and form error. OK only treats the height value as a complete representation of the entire feature.
(3) When the sample size grows larger, CK and OK tend to be unbiased. This is confirmed that when a large sample is used, the distribution of f is centered around the actual flatness error.
(4) CK suffers from not having sufficient information when the simulated sample is small. Some authors point out that a small sample size is not sufficient [9,39]. To a smaller degree, insufficient information from a small sample generally leads to much more uncertainty.

5 Case Study

5.1 Case Study I

5.1.1 Experimental Setup. Machining surfaces for this case is the engine cylinder block top surfaces (see Fig. 8). The engine block was machined under closely supervised conditions to ensure that no anomalous problems with milling process occur. The material of the engine block is cast iron FC250. The milling process was carried out using an EX-CELL-O machining center and a CBN milling cutter with a diameter of 200 mm. Quaker 370 KLG cutting fluid was used. The cutting speed was 816.4 m/min, the depth of cut was 0.5 mm, and feed rate was 3360 mm/min.

The engine block surface was measured using a CMM and $N = 1000$ points to an area of 326.5 mm × 174 mm was acquired. The height deviations are from −80 μm to 80 μm. Figure 9 shows artificial surface with sampling data points.

The tool vibration is considered as one of most important influence factors during the machining process for the surface flatness error estimation. Therefore, vibration is taken into consideration by CK in this case study.

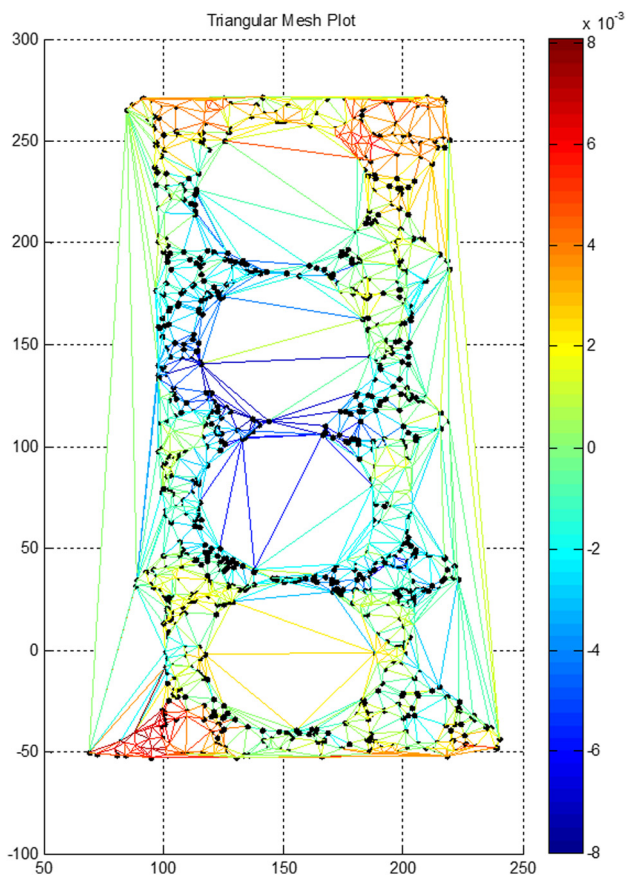

Fig. 9 Color-coded image of the engine block face with triangular mesh plot

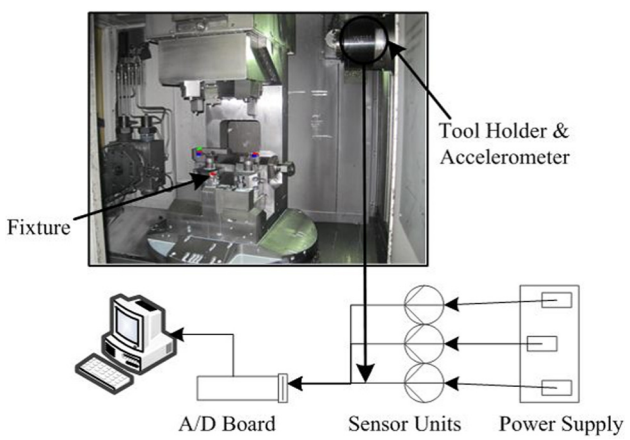

Fig. 10 Hardware setup for milling and the schematic for vibration data collection

Table 2 Basic descriptive statistics for sampling data points

Basic descriptive statistics	Height	Height after normalization	Vibration after normalization
Sample size	1000	1000	1000
Minimum	−0.0080	−3.0311	−1.2653
Maximum	0.0081	3.1394	3.7384
Median	-2×10^{-4}	−0.0417	−0.2152
Mean	-9.13×10^{-5}	8.0158×10^{-17}	4.1178×10^{-15}
Standard deviation	0.0026	1.0005	1.0005
Coefficient of variation	−28.5922	1.2482×10^{16}	2.4297×10^{14}
Skewness	0.1782	0.1782	1.0139
Kurtosis	3.1109	3.1109	3.5753

Table 3 Parameters of theoretical variogram and cross-variogram

Type	Variogram	Sill ($C_0 + C_1$)	Nugget (C_0)	Range (a)	Structural effects ratio (%)
Variogram of height	Spherical model	1.3839	0.1644	197.4504	88.12
	Exponential model	2.0492	0.1330	495.6395	93.51
Variogram of vibration	Spherical model	1.1360	0.4449	114.1963	60.84
	Exponential model	1.0198	0.0383	55.6967	96.24
Cross-variogram of height and vibration	Spherical model	2.1535	0.4066	159.9849	81.12
	Exponential model	2.4396	0.2478	240.0733	89.84

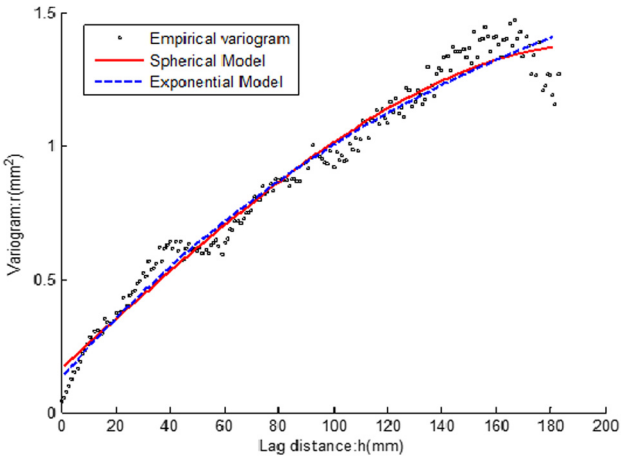

Fig. 11 Theoretical variogram of height in spherical model and exponential model

Table 4 Comparison result with other spatial interpolation methods

	TIN	IDW	OK	CK
ME	−0.08679	−0.05356	−0.03659	−0.00834
MSE	0.3057	0.2895	0.1889	0.1342
AKSE	—	—	0.4946	0.4215
MSPE	—	—	−0.08148	−0.04880
RMSPE	—	—	0.8186	0.8552

The vibration data collection system was comprised of the accelerometer sensors from which signals are amplified, converted to digital data, and processed using Windows-based software. Figure 10 depicts the hardware setup for milling process and the schematic for vibration data collection. The accelerometer sensors are JX20 Eddy current displacement sensors, which were mounted on the shank of the tool holder.

5.1.2 Data Preprocessing. Basic sample descriptive statistics of surface height values are given in Table 2. Since the height and the vibration signal are measured on different scales and units, it

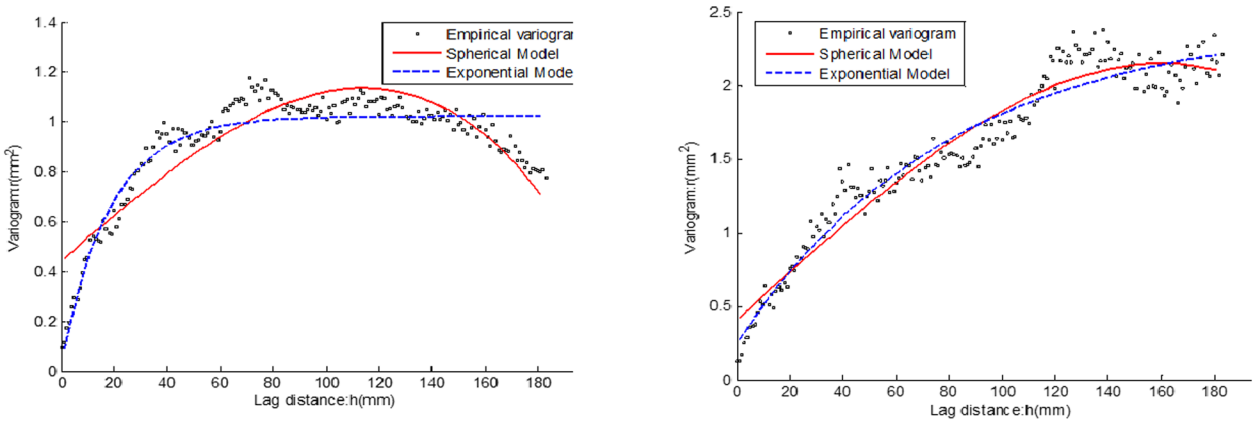

(*a*) (*b*)

Fig. 12 Variogram of vibration and cross-variogram of height and vibration

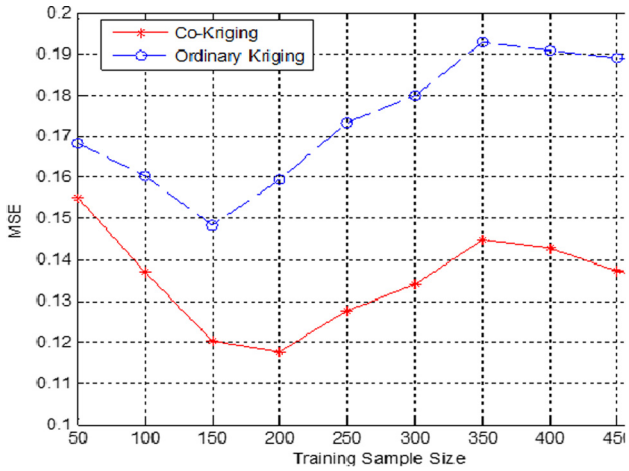

Fig. 13 MSE comparisons between CK and OK estimation

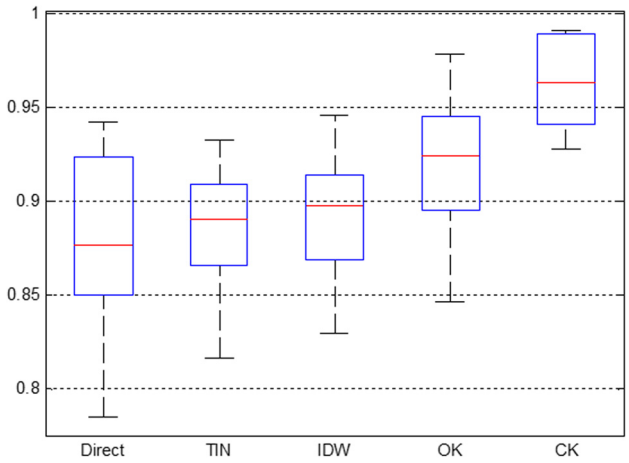

Fig. 14 Box–whisker plot of flatness error estimation by different methods

is necessary to take these data values into the same measuring scales. Data normalization method, which adjusts values measured on different scales to a notionally common scale, is applied to deal with this problem. The intention is that these normalized values allow the comparison of corresponding normalized values in a way that eliminates the effects of certain gross influences. Table 2 also shows the descriptive statistics for the height and vibration after normalization.

The data is normalized according to the below equation:

$$Y = \frac{X - \bar{X}}{s} \tag{19}$$

where $\bar{X}$ is the mean of sample, and s is the standard deviation of sample.

5.1.3 *Results and Discussion*

5.1.3.1 Comparison analysis of spatial correlation. The spatial correlation theory treats variograms as a measure of variability between measured points instead of the Euclidian distance. The empirical variogram is computed as half the average squared difference on varied lag distance between the data pairs. As shown in Fig. 11, the dots characterize the empirical variogram of surface height computed from the 1000 sampled data points.

The fitting process with LS method is used to obtain quantified spatial correlation and theoretical variogram. In Eq. (9), the parameters of spherical model are achieved as $[C_0 + C_1, C_0, a] = [1.3839, 0.1644, 197.4504]$. In Eq. (10), the parameters of the exponential model are achieved as $[C_0 + C_1, C_0, a] = [2.0492, 0.1330, 495.6395]$. Figure 11 also shows the spherical and exponential models fitting result for the variogram of surface height.

In this case, the spatial variability is assumed to be identical in all directions, variogram value only increases with the separated distance. It means that two locations close to each other on the surface are more alike, and thus their squared difference is smaller than those that are further apart. From Table 3, the variogram of the height value reaches a maximum at 197 mm for the spherical model and at 495 mm for the exponential model before dipping and fluctuating around a sill value. The structural effect ratio in exponential model, compared with the spherical model, has the larger value, which means that the spatial correlation between sample points fitted by exponential model is stronger. Therefore, the predictive value of height by Kriging or CK may theoretically be achieved with optimal minimum error.

The vibration signal value is similarly established using theoretical variogram in spherical and exponential models. Figure 12 shows the fitted line for the variograms of the vibration signal value and the cross-variogram of height and vibration. Figure 12(*a*) is the theoretical variogram of vibration in spherical model and exponential model, and Fig. 12(*b*) is the theoretical cross-

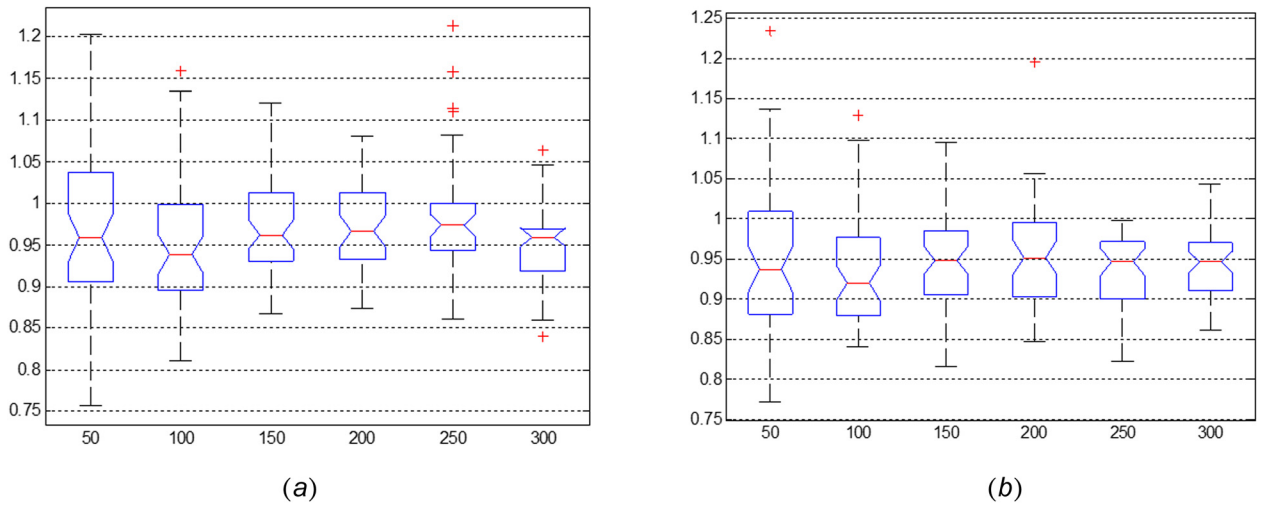

(*a*) (*b*)

Fig. 15 Box–whisker plot of flatness error estimation comparison by different sample size: (*a*) CK and (*b*) OK

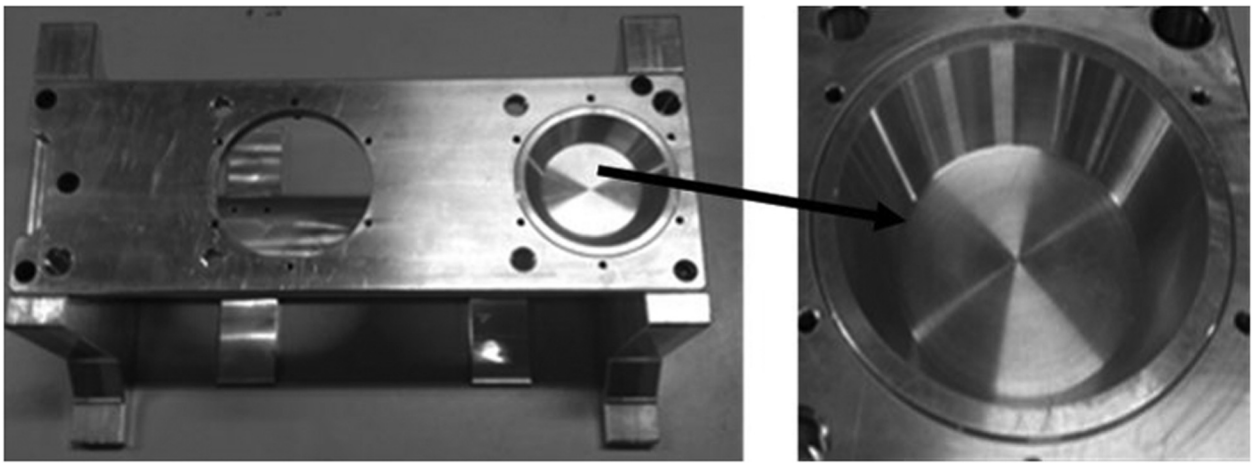

Fig. 16 The workpiece for case study II

variogram of height and vibration in exponential and spherical model.

5.1.3.2 Comparison analysis with other spatial interpolation methods. To better understand how different interpolation methods perform, the height values of 500 data points are estimated in sequence. The difference is examined between the known data and the predicted data using cross validation criteria: mean error (ME), mean square error (MSE), average of Kriging standard error (AKSE), mean standardized prediction error (MSPE), and root mean square standardized prediction error (RMSPE)

$$\mathrm{ME} = \frac{1}{n}\sum_{i=1}^{n}\left[z^*(s_i) - z(s_i)\right] \tag{20}$$

$$\mathrm{MSE} = \frac{1}{n}\sum_{i=1}^{n}\left[z^*(s_i) - z(s_i)\right]^2 \tag{21}$$

$$\mathrm{AKSE} = \sqrt{\frac{1}{n}\sum_{i=1}^{n}\sigma^2(s_i)} \tag{22}$$

$$\mathrm{MSPE} = \frac{1}{n}\sum_{i=1}^{n}\frac{Z^*(s_i) - Z(s_i)}{\sigma(s_i)} \tag{23}$$

$$\mathrm{RMSPE} = \sqrt{\frac{1}{n}\sum_{i=1}^{n}\left[\frac{Z^*(s_i) - Z(s_i)}{\sigma(s_i)}\right]^2} \tag{24}$$

where n is the training sample size, $z(s_i)$ is the true height value, $z^*(s_i)$ is the predicted value, and the corresponding Kriging standard error $\sigma(s_0)$.

The calculated ME is a weak diagnostic for Kriging because it is insensitive to inaccuracies in the variogram. The value of ME also depends on the scale of the data, and is standardized through dividing by the Kriging variance to form the MSPE. An accurate model would have an MSPE close to zero. If the model for the variogram is accurate, then the MSE should equal the Kriging variance, so the RMSPE should equal to one. If the RMSPE is greater than one, then the variability in the predictions is underestimated, and vice versa. AKSE is calculated by the Kriging error variance, which reflects the precision of estimation.

Table 4 shows the comparison result after spatial interpolation by 500 estimated points. Since TIN and IDW methods do not have estimation variance error, criteria MSPE and RMSPE cannot be obtained for them. From Table 4, some findings are obtained

(1) The unmeasured point can be estimated by nearest measured points using traditional interpolation methods like TIN and IDW, but the result of estimation is less precise than the Kriging methods. The indices of ME and MSE for TIN and IDW are larger than that for the Kriging methods. This is because the number of measured points used for estimation by TIN and IDW is limited and the weights of these measured points are specially fixed.
(2) In comparison with different spatial statistics methods, Kriging method can obtain much more accurate estimation with smaller ME and MSE. Moreover, multivariate CK method considering the machining conditions has a more

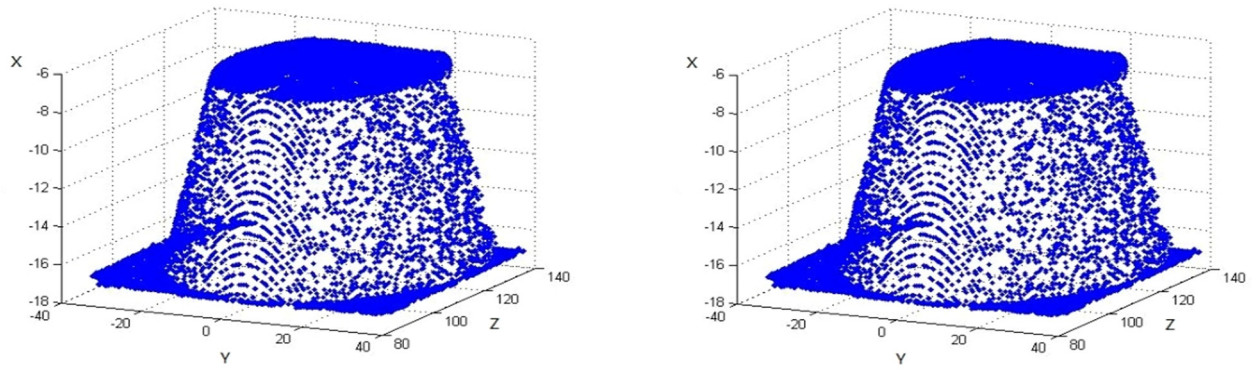

Fig. 17 Curved surface of the workpieces: (*a*) curved surface with upper and lower plane surfaces and (*b*) curved surface

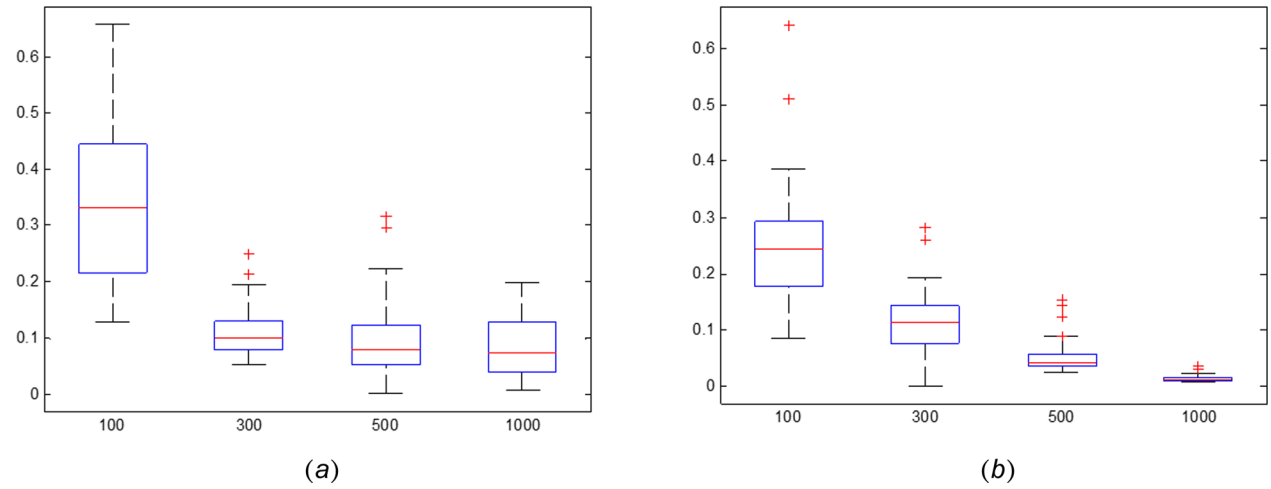

Fig. 18 Box–whisker plot of MSE comparison by different sample size: (*a*) OK and (*b*) CK

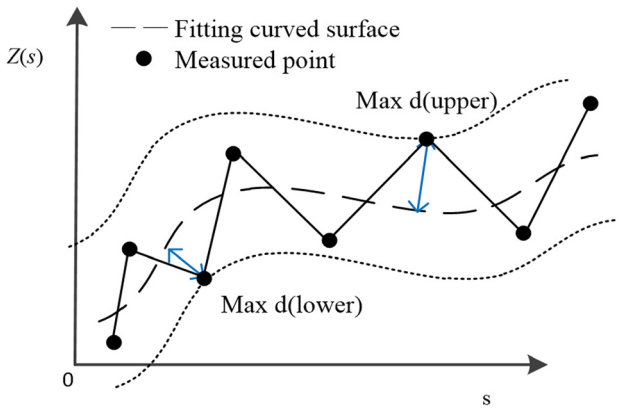

Fig. 19 Diagram of form error estimation for curved surface

Table 5 Comparison result of cross validation by OK and CK for case study II

	OK	CK
ME	0.1084	0.0614
MSE	0.3387	0.2587
AKSE	2.4255	1.7615
MSPE	0.0391	0.0165
RMSPE	0.2233	0.3585

accurate estimation by comparing the results of MSPE and RMSPE. According to AKSE, calculated by Kriging error variance, it indicates the uncertainty of the estimation by Kriging methods. Apparently CK has a much more reliable estimation.

Furthermore, Fig. 13 shows the comparison between CK with vibration signal and OK with different training sample size. According to the average values of MSE in different numbers of points, CK achieves lower MSE value, which means CK is much more valid for estimating the height value taking vibration into account. On the other hand, with the increasing training sample size, the MSE decreases. When it reaches a specified number of training sample points (150 for OK and 200 for CK), the MSE increases. This phenomenon indicates that appropriate training sample size can reach the most precise estimation by Kriging methods. So Kriging method is also applied to decide the appropriate inspection samples and the measure sample size.

5.1.3.3 Comparison analysis of flatness error estimation with other methods. The flatness errors of the engine block surface were calculated using LS method. The form error of the real height value by 600 measured points is treated as true flatness error, and the general flatness error is calculated using interpolation methods: TIN, IDW, OK, and CK. The inspection process is conducted using 100 sample points from this surface based on a random sampling method, and then interpolation methods are applied to estimate 500 locations in sequence and generate an artificial surface to calculate the flatness error. The 100 sample points are used to calculate the flatness error through the direct method.

The flatness error calculated by CK is 0.01339, which is closer to the true value 0.01336, compared with OK with exponential model (0.01328) and with spherical model (0.01347). Since we use a rectangular grid to represent the predicted surface and calculate the flatness error, the results could be low when the points do not capture the minimum and maximum points. Estimated flatness error is smaller by OK with the exponential model.

Figure 14 shows the box–whisker plot of the flatness error estimation by different spatial interpolation methods. Hundred sample points are randomly chosen for 50 times to repeat the flatness error estimation by Direct, TIN, IDW, OK, and CK methods. Obviously, CK performs better in flatness error estimation which is more than 97% of the real value, meanwhile for OK, the percentage is below 95%.

Figure 15 indicates the flatness error estimation by different sample sizes by OK and CK methods. When the sample size is

Table 6 Comparison result of form error estimation by OK and CK for case study II

	Real	Direct			OK	CK
Sample size	7661	100	500	1000	100 + 7561[a]	100 + 7561[a]
Form error	1.2713×10^{-4}	7.3301×10^{-5}	7.5525×10^{-5}	7.9324×10^{-5}	9.6079×10^{-5}	9.9355×10^{-5}
Ratio	100%	57.6583%	59.4077%	62.3960%	75.5754%	78.1523%

[a]100 + 7561 indicates that 100 initial measured points with 7561 estimated points by OK or CK method.

larger, CK and OK tend to be unbiased and CK has a greater convergence speed.

5.2 Case Study II

5.2.1 Experimental Setup. Machining surfaces for this case study is curved surfaces (see Fig. 16). Figure 17 shows an artificial surface with sampling data points.

The height values Z of the curved surface are measured from −40 mm to 40 mm. Around 7661 points are measured offline on the curved surface as the true value for the form error estimation. These 7661 measured points are characterized by three dimensions x, y, and z, and the corresponding vibration signal values are obtained by the sensor online during the machining process.

5.2.2 Results and Discussion

5.2.2.1 Comparison analysis with other spatial interpolation methods. On the curved surface, 100 points with three dimensions measured offline and with vibration signal measured online are randomly selected as the measured values. OK and CK methods are applied to estimate the height value Z for the resting 7561 locations. The real height values and the estimated height values by OK and CK are calculated by the cross-validation criteria: ME, MSE, AKSE, MSPE, and RMSPE. Table 5 shows the result of cross-validation criteria values by OK and CK methods.

Obviously, the CK method considering machining conditions vibration signal can make much more precise estimation. ME, MSE, and MSPE of CK are closer to 0 than those of OK. The uncertainty of Kriging error variance AKSE of CK is less than that of OK, which means the precision of estimation. But the RMSPE of OK and CK is less than 1, which means the sample size of initial measured points for estimation is not enough. It needs much more information for Kriging estimation.

Figure 18 shows the box–whisker plot result of cross validation criteria MSE by OK and CK estimation with a different initial sample size. With the increasing of initial sample size for Kriging estimation, the MSE tends to 0. And for CK method, the speed of convergence is much more higher than that for OK method.

5.2.2.2 Comparison analysis of form error estimation with other methods. For the curved surface, the form error estimation is using the MinMax method introduced by Yang and Jackman [57]. It is calculated by the sum of the maximum distance between the upper or lower measured points and the fitting curved surface (see Fig. 19), which means the minimum distance between the two enveloping surfaces along the fitting curved surface.

Table 6 shows the comparison of form error estimation by direct method, OK and CK method for the curved surface. The form error estimation of the 7661 measured points is regarded as the true value. The direct method chooses randomly 100, 500, 1000 measured points with three dimensions for the form error estimation. For OK and CK, 100 measured points are randomly chosen for estimation of height values Z in the remaining 7561 locations. The ratio is calculated by the form error of direct, OK, or CK method and that of real measured points.

From Table 6, we observe that

(1) With the increase of initial sample size of measured points used to form error estimation, the precision grows from 57% to 62%. But the rate of growth is limited according to the growth of sample size. However, the growth of sample size is at the cost of the measuring cost and efficiency.
(2) The spatial interpolation method can greatly increase the precision of the form error estimation from 57% to 75% even though the number of initial measured points remains low. The improvement for form error estimation is considerable and the measurement cost is reduced.
(3) The proposed multivariate spatial interpolated method still can improve the estimation precision by 2.58% compared to the OK method. This improvement is not large but of great importance for the form error estimation in the manufacturing process.

6 Conclusions

A novel method based on multivariate spatial statistics is developed for more accurate form error estimation. In order to decrease the deviation between the real values and the estimated values, the machining condition data measured online impacting the surface are taken into account. Compared to univariate spatial Kriging method, the multivariate spatial prediction method CK, concerning multiple parameters with different spatial correlations, performs better for the form error estimation. The spatial correlation on product surface is characterized by appropriate variogram and cross-variogram.

Through analyzing the simulation cases, CK considering vibration influence could improve the accuracy of flatness error estimation by 10% over OK without considering vibration. For the case studies, the plane product surface and curved product surface are both illustrated to validate the proposed multivariate spatial statistics CK method. The flatness error estimation on the plan surface by CK also outperforms 10% by direct or TIN/IDW method, and 3–5% by OK. For the form error estimation on the curved surface, CK considering machining conditions can greatly improve the prediction up to 20% comparing with the direct method and also perform better than OK.

Acknowledgment

This work was supported by the National Natural Science Foundation of China (Grant No. 51275558), State Key Lab of Mechanical System and Vibration program (Grant No. MSVZD201503), and Shanghai Rising-Star Program (Grant No. 13QA1402100).

Appendix

The variance and covariance of the parameters Z_1 and Z_2 at locations s and $s+h$ are described as

$$C_{11}(h) = E[\{Z_1(s) - \mu_1\}\{Z_1(s+h) - \mu_1\}] \tag{A1}$$

$$C_{22}(h) = E[\{Z_2(s) - \mu_2\}\{Z_2(s+h) - \mu_2\}] \tag{A2}$$

$$C_{12}(h) = E[\{Z_1(s) - \mu_1\}\{Z_2(s+h) - \mu_2\}] \tag{A3}$$

where μ_1 and μ_2 are the mean of parameters Z_1 and Z_2.

Therefore, the theoretical calculation of covariance based on limited measured points is described as

$$C^*{}_{12}(h) = \frac{1}{2N(h)}\sum_{i=1}^{N(h)}\{z_1(s_i)z_2(s_i+h)\} - \frac{1}{2N(h)}\sum_{i=1}^{N(h)} z_1(s_i) \times \frac{1}{2N(h)}\sum_{i=1}^{N(h)} z_2(s_i+h) \tag{A4}$$

According to the calculation process of covariance, the variogram and co-variogram are constructed as

$$\gamma_{11}(h) = \frac{1}{2}E\left[\{Z_1(s) - Z_1(s+h)\}^2\right] \tag{A5}$$

$$\gamma_{22}(h) = \frac{1}{2}E\left[\{Z_2(s) - Z_2(s+h)\}^2\right] \tag{A6}$$

$$\gamma_{12}(h) = \frac{1}{2}E\left[\{Z_1(s) - Z_1(s+h)\}\{Z_2(s) - Z_2(s+h)\}\right] \tag{A7}$$

And the theoretical co-variogram is calculated

$$\gamma^*{}_{12}(h) = \frac{1}{2N(h)} \sum_{i=1}^{N(h)} \{z_1(x_i) - z_1(x_i + h)\}\{z_2(x_i) - z_2(x_i + h)\} \tag{A8}$$

So the co-variogram is constructed as

$$\gamma_{AB}(h) = \frac{1}{2N_n{}^{AB}(h)} \sum_{i,j \in N_n{}^{AB}(h)} \left[A(s_i) - A(s_j)\right]\left[B(s_i) - B(s_j)\right], \quad \times h \in R^d, A, B \in \{Z, V_t\}$$

References

[1] Du, S., Liu, C., and Xi, L., 2015, "A Selective Multiclass Support Vector Machine Ensemble Classifier for Engineering Surface Classification Using High Definition Metrology," ASME J. Manuf. Sci. Eng., **137**(1), p. 011003.

[2] Du, S., Liu, C., and Huang, D., 2014, "A Shearlet-Based Separation Method of 3D Engineering Surface Using High Definition Metrology," Precis. Eng., **40**, pp. 55–73.

[3] Du, S., Huang, D., and Wang, H., 2015, "An Adaptive Support Vector Machine-Based Workpiece Surface Classification System Using High Definition Metrology," IEEE Trans. Instrum. Meas., **64**(10), pp. 2590–2604.

[4] Wang, M., Xi, L., and Du, S., 2014, "3D Surface Form Error Evaluation Using High Definition Metrology," Precis. Eng., **38**(1), pp. 230–236.

[5] Wang, M., Ken, T., Du, S., and Xi, L., 2015, "Tool Wear Monitoring of Wiper Inserts in Multi-Insert Face Milling Using 3D Surface Form Indicators," ASME J. Manuf. Sci. Eng., **137**(3), p. 031006.

[6] Nguyen, H., Wang, H., and Hu, S. J., 2013, "Characterization of Cutting Force Induced Surface Shape Variation Using High-Definition Metrology," ASME J. Manuf. Sci. Eng., **135**(4), p. 041014.

[7] Guo, P., Lu, Y., Pei, P., and Ehmann, K. F., 2014, "Fast Generation of Micro-Channels on Cylindrical Surfaces by Elliptical Vibration Texturing," ASME J. Manuf. Sci. Eng., **136**(4), p. 041008.

[8] Rao, P., Bukkapatnam, S., Beyca., O., Kong, Z., and Komanduri, R., 2014, "Real-Time Identification of Incipient Surface Morphology Variations in Ultra-precision Machining Process," ASME J. Manuf. Sci. Eng., **136**(2), p. 021008.

[9] Zhu, X., Ding, H., and Wang, M., 2004, "Form Error Evaluation: An Iterative Reweighted Least Squares Algorithm," ASME J. Manuf. Sci. Eng., **126**(3), pp. 535–542.

[10] Raghunandan, R., and Rao, P. V., 2007, "Selection of an Optimum Sample Size for Flatness Error Estimation While Using Coordinate Measuring Machine," Int. J. Mach. Tools Manuf., **47**(3–4), pp. 477–482.

[11] Badar, M. A., Raman, S., and Pulat, P. S., 2005, "Experimental Verification of Manufacturing Error Pattern and Its Utilization in Form Tolerance Sampling," Int. J. Mach. Tools Manuf., **45**(1), pp. 63–73.

[12] Dowling, M., Griffin, P., Tusi, K., and Zhou, C., 1997, "Statistical Issues in Geometric Feature Inspection Using Coordinate Measuring Machines," Technometrics, **39**(1), pp. 3–17.

[13] Yan, Z., and Menq, C., 1995, "Uncertainty Analysis for Coordinate Estimation Using Discrete Measurement Data," ASME International Mechanical Engineering Congress and Exposition, Vol. 1, San Francisco, CA, Nov. 12–17, pp. 595–616.

[14] Yeh, K. M., Ni, J., and Hu, S., 1994, "Adaptive Sampling and Identification of Feature Deformation for Tolerance Evaluation Using Coordinate Measuring Machines," S. M. Wu, Manufacturing Research Laboratory, Department of Mechanical Engineering and Applied Mechanics, University of Michigan, Ann Arbor, MI, Technical Report.

[15] Yang, B., and Menq, C., 1993, "Compensation for Form Error of End-Milled Sculptured Surfaces Using Discrete Measurement Data," Int. J. Mach. Tools Manuf., **33**(5), pp. 725–740.

[16] Henke, R., Summerhays, K., Baldwin, J., Cassou, R., and Brown, C., 1999, "Methods for Evaluation of Systematic Geometric Deviations in Machined Parts and Their Relationships to Process Variables," Precis. Eng., **23**(4), pp. 273–292.

[17] Cho, N., and Tu, J., 2001, "Roundness Modeling of Machined Parts for Tolerance Analysis," Precis. Eng., **25**(1), pp. 35–47.

[18] Desta, M. T., Feng, H. Y., and Ou Yang, D., 2003, "Characterization of General Systematic Form Errors for Circular Features," Int. J. Mach. Tools Manuf., **43**(11), pp. 1067–1078.

[19] Xia, H., Ding, Y., and Wang, J., 2008, "Gaussian Process Method for Form Error Assessment Using Coordinate Measurements," IIE Trans., **40**(10), pp. 931–946.

[20] Walker, E., and Wright, S. P., 2002, "Comparing Curves Using Additive Models," J. Qual. Technol., **34**(1), pp. 118–129.

[21] Whittle, P., 1954, "On Stationary Processes in the Plane," Biometrika, **41**(3/4), pp. 434–449.

[22] Sayles, R. S., and Thomas, T. R., 1977, "The Spatial Representation of Surface Roughness by Means of the Structure Function: A Practical Alternative to Correlation," Wear, **42**(2), pp. 263–276.

[23] Colosimo, B. M., and Semeraro, Q., 2008, "Statistical Process Control for Geometric Specifications: On the Monitoring of Roundness Profiles," J. Qual. Technol., **40**(1), pp. 1–18.

[24] Murthy, T. E. R., and Abdin, S. Z., 1980, "Minimum Zone Evaluation of Surfaces," Int. J. Mach. Tools Des. Res., **20**(2), pp. 123–136.

[25] Wang, Y., 1992, "Minimum Zone Evaluation of Form Tolerances," Manuf. Rev., **5**(3), pp. 213–220.

[26] Kannda, T., and Suzuki, S., 1993, "Evaluation of Minimum Zone Flatness by Means of Non-Linear Optimization Technique and Its Verification," Precis. Eng., **15**(2), pp. 93–99.

[27] Suriano, S., Wang, H., Shao, C., Hu, S. J., and Sekhar, P., 2015, "Progressive Measurement and Monitoring for Multi-Resolution Data in Surface Manufacturing Considering Spatial and Cross Correlations," IIE Trans., **47**(10), pp. 1033–1052.

[28] Li, J., and Heap, A. D., 2008, *A Review of Spatial Interpolation Methods for Environmental Scientists*, Vol. 23, Geoscience Australia, Canberra, Australia, pp. 137–145.

[29] Chen, X., Ankenman, B. E., and Nelson, B. L., 2013, "Enhancing Stochastic Kriging Metamodels With Gradient Estimators," Oper. Res., **61**(2), pp. 512–528.

[30] Kleijnen, J. P. C., and Mehdad, E., 2014, "Multivariate Versus Univariate Kriging Metamodels for Multi-Response Simulation Models," Eur. J. Oper. Res., **236**(2), pp. 573–582.

[31] Kleijnen, J. P. C., 2009, "Kriging Metamodeling in Simulation: A Review," Eur. J. Oper. Res., **192**(3), pp. 707–716.

[32] Yang, T. H., and Jackman, J., 2000, "Form Error Estimation Using Spatial Statistics," ASME J. Manuf. Sci. Eng., **122**(2), pp. 262–272.

[33] Morimoto, Y., Suzuki, N., Kaneko, Y., and Isobe, M., 2014, "Vibration Control of Relative Tool-Spindle Displacement for Computer Numerically Controlled Lathe With Pipe Frame Structure," ASME J. Manuf. Sci. Eng., **136**(4), p. 044502.

[34] Weckenmann, A., Heinrichowski, M., and Mordhorst, H., 1991, "Design of Gauges and Multipoint Measuring Systems Using Coordinate Measuring-Machine Data and Computer Simulation," Precis. Eng., **13**(3), pp. 203–207.

[35] Yan, D., Popplewell, N., Balkrishnan, S., and Kaye, J. E., 1996, "On-Line Prediction of Surface Roughness in Finish Turning," Eng. Des. Autom., **2**(2), pp. 115–126.

[36] Chen, L., 2008, "Study on Prediction of Surface Quality in Machining Process," J. Mater. Process. Technol., **205**(1–3), pp. 439–450.

[37] Roth, J. T., Mears, L., Djurdjanovic, D., Yang, X., and Kurfess, T., 2007, "Quality and Inspection of Machining Operations: Review of Condition Monitoring and CMM Inspection Techniques," ASME International Conference on Manufacturing Science and Engineering, Vol. 10, pp. 15–18.

[38] Benardo, S. P. G., and Vosniakos, G. C., 2003, "Predicting Surface Roughness in Machining a Review," Int. J. Mach. Tools Manuf., **43**(8), pp. 833–844.

[39] Dowling, M., Griffin, P., Tsui, K., and Zhou, C., 1995, "A Comparison of the Orthogonal Least Square and Minimum Enclosing Zone Methods for Form Error Estimation," Manuf. Rev., **8**, pp. 120–134.

[40] Matheron, G., 1973, "The Intrinsic Random Functions, and Their Applications," Adv. Appl. Probab., **5**(3), pp. 439–468.

[41] Cressie, N., 1993, *Statistics for Spatial Data, Revised Edition*, Wiley, New York.

[42] Zhang, R. D., 2005, *Spatial Variogram Theory and Its Application*, Science and Technology Press, Beijing.

[43] Deutsch, C. V., and Journel, A. G., 1992, *GSLIB—Geostatistical Software Library and User's Guide*, Oxford University Press, New York.

[44] Isaaks, E. H., and Srivastava, R. M., 1989, *An Introduction to Applied Geostatistics*. Oxford University Press, New York.

[45] Goovaerts, P., 1997, *Geostatistics for Natural Resources Evaluation*, Oxford University Press, New York.

[46] Ahmed, S., and Marsity, G. D., 1987, "Comparison of Geostatistical Methods for Estimating Transmissivity Using Data on Transmissivity and Specific Capacity," Water Resour. Res., **23**(9), pp. 1717–1737.

[47] Gelfand, A. E., Diggle, P., Guttorp, P., and Fuentes, M., eds., 2010, *Handbook of Spatial Statistics*, CRC Press, Boca Raton, FL.

[48] Kennedy, M. C., and O'Hagan, A., 2000, "Predicting the Output From a Complex Computer Code When Fast Approximations are Available," Biometrika, **87**(1), pp. 1–13.

[49] Zhou, Q., Qian, P. Z., and Zhou, S., 2011, "A Simple Approach to Emulation for Computer Models With Qualitative and Quantitative Factors," Technometrics, **53**(3), pp. 266–273.

[50] Qian, P. Z., and Wu, C. J., 2008, "Bayesian Hierarchical Modeling for Integrating Low-Accuracy and High-Accuracy Experiments," Technometrics, **50**(2), pp. 192–204.

[51] Clark, I., Basinger, K. L., and Harper, W. V., 1987, "A Novel Approach to Co-Kriging," Conference on Geostatistical, Sensitivity, and Uncertainty Methods for Ground-Water Flow and Radionuclide Transport Modeling, San Francisco, CA, pp. 473–493.

[52] Rehman, S. U., and Shapiro, A., 1996, "An Integral Transform Approach to Cross-Variograms Modeling," Comput. Stat. Data Anal., **22**(3), pp. 213–233.

[53] Armstrong, M., and Diamond, P., 1984, "Testing Variograms for Positive-Definiteness," Math. Geol., **16**(4), pp. 407–421.

[54] Myers, D. E., 1994, "Spatial Interpolation: An Overview," Geoderma, **62**(1–3), pp. 17–28.

[55] Myers, D. E., 1982, "Matrix Formulation of Co-Kriging," Math. Geol., **14**(3), pp. 249–257.

[56] Myers, D. E., 1983, "Estimation of Linear Combinations and Co-Kriging," Math. Geol., **13**(5), pp. 633–637.

[57] Yang, T. H., and Jackman, J., 1997, "A Probabilistic View of Problems in Form Error Estimation," ASME J. Manuf. Sci. Eng., **119**(3), pp. 375–382.